

# Damage detection in beam-like structures using static shear energy redistribution

Xi PENG<sup>a,b</sup>, Qiuwei YANG<sup>a,b\*</sup>

<sup>a</sup> School of Civil and Transportation Engineering, Ningbo University of Technology, Ningbo 315211, China

<sup>b</sup> Engineering Research Center of Industrial Construction in Civil Engineering of Zhejiang, Ningbo University of Technology, Ningbo 315211, China

\*Corresponding author. E-mail: yangqiuwei79@gmail.com

© Higher Education Press 2022

**ABSTRACT** In this study, a static shear energy algorithm is presented for the damage assessment of beam-like structures. According to the energy release principle, the strain energy of a damaged element suddenly changes when structural damage occurs. Therefore, the change in the static shear energy is employed to determine the damage locations in beam-like structures. The static shear energy is derived from the spectral factorization of the elementary stiffness matrix and structural deflection variation. The advantage of using shear energy as opposed to total energy is that only a few deflection data points of the beam structure are required during the process of damage identification. Another advantage of the proposed approach is that damage detection can be performed without establishing a structural finite-element model in advance. The proposed technique is first validated using a numerical example with single, multiple, and adjacent damage scenarios. A channel steel beam and rectangular concrete beam are employed as experimental cases to further verify the proposed approach. The results of the simulation and experiment examples indicate that the proposed algorithm provides a simple and effective method for defect localization in beam-like structures.

**KEYWORDS** damage detection, beam structure, strain energy, static displacement variation, energy damage index

## 1 Introduction

During the service period of an engineering structure, material aging, fatigue, cracking, and other damages can occur in the structure owing to environmental corrosion and disaster load. Local damages in a structure reduce the bearing capacity, affect normal use, and lead to the collapse of the structure. Therefore, detection of defects in a structure has attracted significant attention in the past decades in the field of structural safety. Beam-like structures are the most commonly used components in bridges, buildings, and mechanical engineering applications. To avoid engineering accidents, it is necessary to develop effective damage assessment methods for beam-like structures. To this end, many methods have been developed in recent years to detect structural defects using changes in structural response parameters [1–3]. Based on the type of data used, structural damage

diagnosis technology can be classified into two types: dynamic and static. The dynamic-based approach is more mature than the static-based technique because the dynamic test does not affect the normal use of the structure. Currently, dynamic methods mainly use the following dynamic characteristic parameters: velocity or acceleration [4,5], vibration frequency [6–8], mode shapes [9–16], flexibility matrix [17–20], curvature [21–23], moving-load responses [24–26], and modal strain energy [27–29]. Liu et al. [4,5] conducted acceleration-based parameter identification on an airfoil-store system and a fractional-order system using the enhanced response sensitivity algorithm. Messina et al. [6] used the changes in vibration frequencies to assess the position and severity of structural defects. Ashokkumar and Iyengar [7] presented an approach based on partial eigenvalue assignment for structural damage diagnosis. Yang and Wang [8] proposed a natural frequency vector assurance criterion to evaluate the structural damage. In certain cases, the frequency is not sensitive to local

defects in a structure because it corresponds to the vibration characteristic of the entire structure. Therefore, the mode shape of the structural vibration is also employed in structural damage diagnosis. Shi et al. [9] presented an algorithm based on a statistical tool to determine the defect locations using only partial data of the vibration eigenvectors. Ghannadi and Kourehli [10–13] used model reduction and expansion techniques to solve the incomplete measurement problem of vibration modes for damage identification. After comparing various model reduction methods, they concluded that the system equivalent reduction expansion process (SEREP) can obtain the most accurate model condensation results in numerical simulations [10]. Then, they used the SEREP to expand the measured vibration modes and further applied an artificial neural network (ANN) [11,12] or grey wolf optimization algorithm [13] to conduct structural damage identification. As an alternative, they also used the least-squares support vector machine (LS-SVM) [14] to compute the unmeasured vibration mode data using the measured vibration mode data for structural damage detection. Zhu et al. [15] presented a defect-diagnosis technique based on the slopes of the first vibration mode for damage detection in shear buildings. Zhang et al. [16] used the square of the vibration mode as an index to identify the defects in bridge structures. The structural flexibility matrix was observed to be more sensitive to structural damage than the vibration frequency and mode under many conditions. Wu and Law [17] employed the sensitivity of modal flexibility to modify a finite element model for structural damage identification. Di and Law [18] further improved the modal flexibility sensitivity method using a more accurate element stiffness model. Yang [19,20] developed damage identification algorithms via spectral factorization of the structural global and local flexibility matrices. Based on the flexibility matrix, Sung et al. [21] developed a damage diagnosis technique for beam structures using the curvature of the normalized uniform load surface. It was concluded that the curvature-based approach can lead to damage identification via the sole use of the vibration information of the damaged structure. Using Fourier spectral analysis, Yang et al. [22] employed a new curvature-based technique to determine the defect positions in beam structures. Using the wavelet transform technique, Xiang et al. [23] extracted the curvature mode shapes to identify structural defect positions. For bridge structures, the moving load method is also widely used because it can utilize the acquired data when a truck passes through the bridge to perform damage assessment. Khorram et al. [24] investigated the performance of moving-load approaches to determine the beam defect position and extent of damage. The results showed that cracks, whose length exceeded 10% of the beam height, can be successfully identified using the

moving load method. Roveri and Carcaterra [25] proposed a damage assessment algorithm based on the traveling load of bridge structures. They determined that the diagnosis results were affected by the defect position and load moving speed. Cavadas et al. [26] developed a data-driven method based on a moving load to determine defect positions. Their approach was successful in continuously monitoring bridge structures. The strain energy distribution in a structure is closely related to the damage status of the structure. Therefore, energy-based defect assessment algorithms have attracted widespread interest in engineering. Xu et al. [27] proposed a defect assessment method based on strain energy for monitoring the structural health of a long-span cable-stayed bridge. Yi et al. [28] extracted wavelet packet component energies to identify structural damage. Cha and Buyukozturk [29] observed that modal strain energy is highly sensitive to structural defects. Recently, novel optimization algorithms [30–33] have been increasingly implemented for structural damage identification. It is expected that various objective functions and optimization algorithms will significantly affect the quality of damage diagnosis. Ghannadi and Kourehli [30] examined the performance of moth-flame optimization (MFO) in defect diagnosis using an objective function consisting of structural flexibility and natural frequency. Ghannadi and Kourehli [31] investigated the performance of a bio-inspired optimization termed as a salp swarm in damage detection using an objective function based on the natural frequency vector assurance criterion (NFVAC). Ghannadi and Kourehli [32] employed a multiverse optimizer (MVO) and two objective functions to solve damage identification issues. The two objective functions corresponded to the modal assurance criterion (MAC) and modified total modal assurance criterion (MTMAC). Ghannadi and Kourehli first employed the latest methods of the slime mold algorithm (SMA) and marine predators algorithm (MPA) to detect defects in large-scale structures [33]. They also investigated the sensitivity of these objective functions to MAC, MTMAC, and NFVAC. It was determined that the combination of SMA and MTMAC can lead to highly accurate damage diagnosis results. They further proposed an improved SMA (ISMA) to strengthen the ability of the original SMA for diagnosing defects. It has been shown that ISMA exhibits obvious advantages in solving the overall optimization issues. The dynamic method is simple when compared with the static method. However, to date, there are many challenges with this type of method, which should be further examined and resolved. Wang et al. [34] indicated that the main challenges that should be resolved in the dynamic method are as follows: (1) structural stiffness, mass, and damping affect the characteristic vibration parameters of a structure. However, many dynamic methods assume no damping in

the structure and that structural damage has no effect on the mass; (2) for a large structure, it is difficult to accurately measure the modal parameters of structural vibration, particularly the vibration mode shape; (3) certain dynamic damage identification methods require high-order vibration modes to identify structural damage. However, in practice, it is difficult to obtain high-order vibrational modes.

Conversely, the static damage evaluation algorithm exhibits two advantages. First, static displacement data are easy to measure and exhibit high accuracy in practice. Second, the static damage evaluation algorithm is only related to structural stiffness. Thus, in recent years, static damage evaluation algorithms have attracted widespread attention in civil engineering applications. Based on static displacements, Sanayei and Onipede [35] examined an iteration-based optimization approach for updating a structural model. Banan et al. [36,37] compared various static-based damage assessment methods and indicated the problems that should be solved. Using static data, Hjelmstad and Shin [38] developed a combinatorial optimization technique for calculating elementary damage coefficients in a structure. Wang et al. [34] combined vibration frequency sensitivity with static displacement sensitivity to diagnose the damage state of a structure. Chou and Ghaboussi [39] developed a genetic approach for calculating defect coefficients in a structure by employing static displacement data. Bakhtiari-Nejad et al. [40] used the optimal calculation approach to conduct a structural damage assessment by considering the nonlinear characteristics of the static displacement between intact and damaged structures. Chen et al. [41] developed a two-stage defect assessment method based on static-displacement data. First, the grey system theory was employed to determine the damage locations. Second, an optimal approach was used for computing the defect coefficients. Using static data as input parameters, Kouchmeshky et al. [42] developed a coordinated evolutionary optimization algorithm to evaluate the structural defect state more accurately. Abdo [43,44] examined the connection between the static displacement curvature and structural defect location and developed a defect diagnosis approach using the displacement curvature.

The aforementioned static methods are mainly based on the geometric changes due to damage but do not deeply explore the relationship between structural damage and strain energy. In essence, there must be a connection between structural damage and strain energy because the occurrence of damage inevitably leads to energy release in the damaged area. Therefore, damage identification based on the redistribution of static strain energy is an effective and feasible method that should be explored further. To this end, in this study, a static shear energy method is proposed for the defect diagnosis of beam-like structures. In contrast to the existing techniques, the

novelty of the proposed approach is that the static shear energy is defined and used for structural damage identification for the first time. As part of the total energy, the shear energy can be derived from the matrix spectral factorization of the elementary stiffness and the deflection variation of the beam structure. The advantage of using shear energy as opposed to total energy is that only a few deflection data points of the beam structure are required in the process of damage identification. This implies that this new approach can overcome the disadvantage of using rotational displacement data in existing total energy methods. According to the energy release principle, the strain energy of a damaged element changes suddenly when structural damage occurs. Conversely, the damage location in a beam can be determined by searching for the mutation location of static shear energy. In a specific operation, the shear energy variation curve and statistical tool can be used to determine the mutation location visually and quantitatively. Based on the theoretical derivation, the proposed method exhibits another advantage wherein defect diagnosis can be performed without establishing a structural finite element model in advance. This advantage makes the proposed method very simple and fast in terms of calculation. Hence, the defect position in a beam can be determined quickly. A numerical case is used to investigate the applicability of this new approach in detecting single, multiple, and adjacent damages in a beam with and without data noise. Two experimental examples of steel and concrete beams were employed to further validate the damage localization ability of the proposed approach. The general framework of this study is as follows. In Section 2, the fundamentals and key formulae of the static shear energy redistribution approach are described. In Section 3, this new approach is verified via a numerical beam structure with single, multiple, and adjacent defect conditions. In Section 4, a channel steel beam and rectangular concrete beam are employed as experimental cases to validate the proposed approach. Finally, several advantages and limitations of this algorithm for practical engineering applications are summarized in Section 5.

---

## 2 Static shear energy redistribution method

For an intact beam, the static response relationship of the structure is as follows.

$$Ku = f, \quad (1)$$

where  $K$  denotes the overall  $n \times n$  stiffness matrix,  $u$  denotes the static response vector, and  $f$  denotes the vector of static loading. The structural displacement vector  $u$  is measured via a static loading experiment in

engineering practice. Static displacement measurement technology can be classified into two categories: contact and non-contact measurement. Dial indicators and resistance displacement sensors are commonly used as displacement meters for contact measurements. Optical inspection or optoelectronic scanning is a common tool for noncontact measurements. This type of advanced displacement testing equipment includes a high-precision video test system and laser Doppler displacement meter. It is expected that the work due to static loading will be converted into the deformation energy of a structure. From Eq. (1), the work due to  $f$  can be computed as follows.

$$W = f^T \cdot u = u^T K u. \tag{2}$$

According to the finite element model (FEM), matrix  $K$  denotes the sum of all elemental stiffness matrices  $K_i$  ( $i = 1 - N$ ). Thus, Eq. (2) can be rewritten as follows.

$$W = u^T \left( \sum_{i=1}^N K_i \right) u = \sum_{i=1}^N \Omega_i, \tag{3}$$

$$\Omega_i = u^T K_i u, \tag{4}$$

where  $\Omega_i$  is defined as the strain energy of the  $i$ th element. Next, the elemental strain energy  $\Omega_i$  is further decomposed using the spectral decomposition of  $K_i$  for damage detection. From FEM theory,  $K_i$  denotes a rank-deficient matrix for most elements. For example,  $K_i$  ranks one for the truss element and ranks two for the plane beam element. Without loss of generality, the spectral decomposition process of the elemental stiffness matrix is described by taking the plane beam element as an example. As shown in Fig. 1, the stiffness matrix  $K_i^e$  of a plane beam element under a local coordinate system is as follows.

$$K_i^e = \frac{EI}{L^3} \begin{bmatrix} 12 & 6L & -12 & 6L \\ 6L & 4L^2 & -6L & 2L^2 \\ -12 & -6L & 12 & -6L \\ 6L & 2L^2 & -6L & 4L^2 \end{bmatrix}, \tag{5}$$

where  $E$  denotes the Young's elastic modulus,  $L$  denotes the length of the beam element, and  $I$  denotes the inertia moment.

By performing spectral decomposition of the element stiffness matrix  $K_i^e$ , the eigenvalue matrix  $P$  and eigenvector matrix  $\eta^e$  can be obtained as follows.

$$K_i^e = \eta^e P \eta^{eT}, \tag{6}$$

$$P = \begin{bmatrix} \frac{6EI(L^2 + 4)}{L^3} & \\ & \frac{2EI}{L} \end{bmatrix}, \tag{7}$$

$$\eta^e = \begin{bmatrix} \frac{\sqrt{2}}{\sqrt{L^2 + 4}} & 0 \\ \frac{L}{\sqrt{2}\sqrt{L^2 + 4}} & \frac{-1}{\sqrt{2}} \\ -\frac{\sqrt{2}}{\sqrt{L^2 + 4}} & 0 \\ \frac{L}{\sqrt{2}\sqrt{L^2 + 4}} & \frac{1}{\sqrt{2}} \end{bmatrix}. \tag{8}$$

In Eq. (7), it can be observed that the diagonal coefficients of the eigenvalue matrix  $P$  are related to the physical parameters  $E$  and  $I$ . However, eigenvector matrix  $\eta^e$  is independent of these physical parameters. Therefore,  $P$  changes and  $\eta^e$  does not change when a defect occurs. According to Eq. (8), the two column vectors in  $\eta^e$  can be considered as the virtual force vectors applied to the beam element under the local coordinate system as shown in Fig. 2.

Equation (6) can be rewritten by transforming the local coordinates to the global coordinates as follows.

$$K_i = \eta P \eta^T, \tag{9}$$

$$\eta = T_i \eta^e, \tag{10}$$

where  $T_i$  denotes the connection matrix between local and global coordinates. Using Eqs. (9) and (4), we can obtain the following.

$$\Omega_i = (\sqrt{p_{11}} u^T \eta_1)^2 + (\sqrt{p_{22}} u^T \eta_2)^2, \tag{11}$$

where  $p_{11}$  and  $p_{22}$  denote the diagonal coefficients of  $P$ ,  $\eta_1$  and  $\eta_2$  denote the first and second column vectors of  $\eta$ .

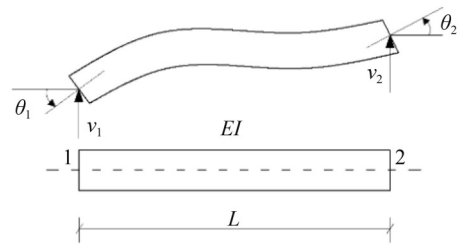


Fig. 1 Beam element with four degrees of freedom.

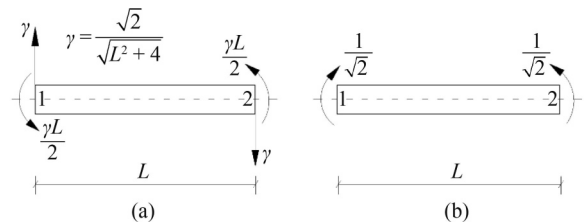


Fig. 2 Virtual force vectors applied on the plane beam element. (a) The first column vector of  $\eta^e$ ; (b) the second column vector of  $\eta^e$ .

From Eqs. (11) and (2), the elemental strain energy  $\Omega_i$  can be divided into two parts, which reflect the shear and bending strain energies. Generally, only the deflection of the beam structure can be obtained in practice because it is difficult to measure the angular displacement. Thus, only the shear strain energy  $\Omega_i^s$  can be calculated using Eq. (11) after removing the rotational DOFs as follows.

$$\Omega_i^s = (\bar{u}^T \xi_i)^2, \tag{12}$$

$$\xi_i = \sqrt{p_{11}} \cdot \bar{\eta}_1, \tag{13}$$

where  $\bar{u}$ ,  $\bar{\eta}_1$  denote the reduced vectors of  $u$ ,  $\eta_1$  after removing the rotational DOF data, and  $\xi_i$  denotes the DOF connected vector of the  $i$ -th beam element. Based on Eqs. (7), (8), and (13), we obtain the following.

$$\xi_i = \frac{2}{L} \sqrt{\frac{3EI}{L}} \cdot (0, \dots, 0, 1, 0, -1, 0, \dots)^T. \tag{14}$$

In Eq. (14), the nonzero coefficients 1 and  $-1$  correspond to the translational DOFs of the beam element. Based on Eq. (14), the DOF-connected vector  $\xi_i$  can be obtained directly from the physical and geometric parameters of the structure without establishing the FEM. Particularly, for an equal-section beam with a uniform mesh, the calculation of the energy damage index is very simple because all the elements in the beam FEM have the same  $E$ ,  $I$ , and  $L$ . For this special case, coefficient  $\frac{2}{L} \sqrt{\frac{3EI}{L}}$  in Eq. (14) can be considered as 1 to further simplify the calculation because the specific value of  $\frac{2}{L} \sqrt{\frac{3EI}{L}}$  does not affect the final damage localization results.

Based on energy release theory, the strain energy of each element of the beam must be redistributed before and after structural damage. Therefore, the strain energy of the damaged element changes suddenly when the

damage occurs. Therefore, a change in the shear strain energy is proposed in this study to determine the positions with defects in the beam structure. To this end, the change in the value of the square root of  $\Omega_i^s$  is used in damage detection for a further simplified calculation as follows.

$$\Delta\Omega_i'' = \xi_i^T \cdot \Delta\bar{u}, \tag{15}$$

where  $\Delta\Omega_i''$  denotes the change in the value of the square root of  $\Omega_i^s$  when a defect occurs, and  $\Delta u_i$  denotes the change in beam deflection. Finally,  $\Delta\Omega_i''$  denotes the energy damage index associated with the  $i$ th beam unit. Equation (14) can considerably simplify the calculation of the energy damage index in Eq. (15). Using Eq. (14), the energy damage index  $\Delta\Omega_i''$  can also be directly calculated from Eq. (15) for damage detection without constructing the structural FEM. By considering the unit number as the abscissa and damage index as the ordinate, the defect position in a structure can be identified via the sudden change in the position of the plotted curve.

The process of the entire algorithm is summarized as follows. Step 1: For each beam element, calculate the DOF-connected vector  $\xi_i$  using Eq. (14). Step 2: Perform static testing on the beam structure and calculate the deflection change  $\Delta\bar{u}$  before and after the damage. Step 3: The elemental damage index  $\Delta\Omega_i''$  is calculated using Eq. (15). Step 4: Draw the damage index curve and identify damage. A flow sheet for this new approach is presented in Fig. 3.

### 3 Numerical verification of the proposed method

The concrete beam presented in Fig. 4 is employed as an example to describe the process and effect of damage identification using the shear energy technique. MATLAB software was employed to implement the presented algorithm for this numerical example on a

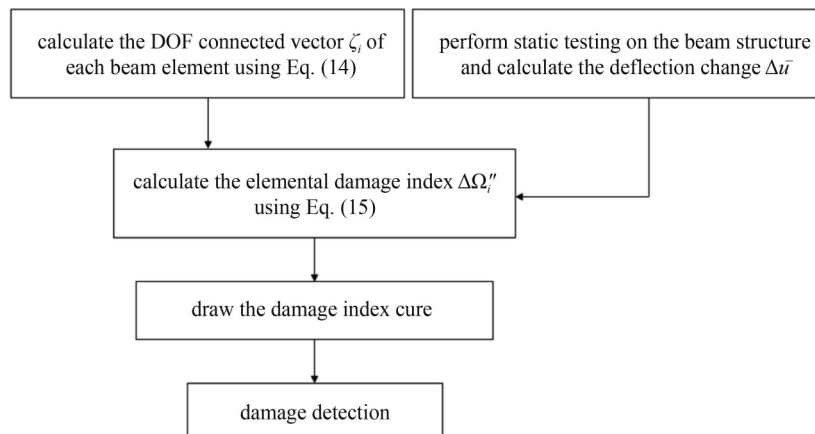


Fig. 3 Flowchart of the static shear energy method.

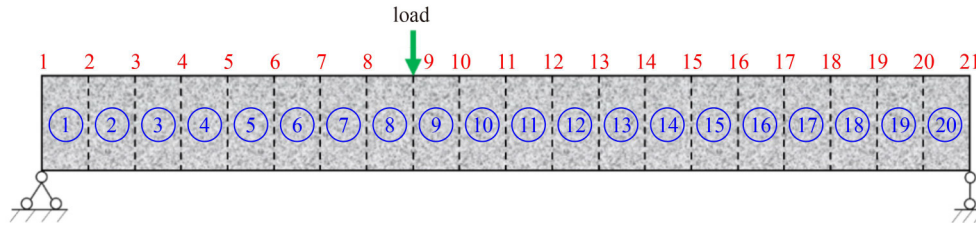


Fig. 4 Element and node numbers for the numerical beam.

computer. The material of the model was assumed as isotropic and linearly elastic. The type of element corresponded to a two-node Bernoulli–Euler plane beam element. As shown in Fig. 4, this beam is equally divided into 20 segments, and each segment length is  $\Delta x = 0.1$  m. The main physical and geometric parameters of the beam structure are as follows. The elastic modulus and density of the material are  $E = 27$  GPa and  $\rho = 2650$  kg/m<sup>3</sup>, respectively. The area and inertia moment of the beam cross-section are  $A = 0.06$  m<sup>2</sup> and  $I = 4.5 \times 10^{-4}$  m<sup>4</sup>, respectively. Table 1 lists the six damage conditions simulated in this example. It is assumed that the vertical displacements at the nodes in Fig. 4 are measured when a concentrated force of 200 kN is applied at node 9. In this example, numerical simulation deflection data are employed to simulate the actual measured deflection parameters for damage identification. Using the deflection variation data due to damage, the values of the elemental damage index  $\Delta\Omega'_i$  can be directly calculated using Eqs. (14) and (15). Table 2 and Fig. 5 present the calculated results for damage cases 1–4 without data noise.

According to Eq. (15), the energy damage index  $\Delta\Omega'_i$  corresponds to 0 because the deflection change  $\Delta\bar{u}$  is zero for an intact structure with no damage. This implies that the damage index graph is a horizontal line, i.e., the  $x$ -axis itself, for the intact case. The quantitative damage assessment is described as follows. From Table 2, it can be observed that the damage indices of beam elements 1–9 are equal, and the damage indices of beam elements 11–20 are also equal. Only the damage index of element 10 showed a mutation. This implies that the energy damage index of element 10 significantly differs from that of the adjacent elements. Therefore, unit 10 can be determined as a damaged unit according to the sudden change in the damage index. Furthermore, Fig. 5 illustrates more clearly that element 10 is a damaged element based on the perspective of the curve. As shown in Fig. 5, the damage index curve corresponding to the damaged structure is not a horizontal line, but a stepped broken line. The damage indices form two parallel lines with the exception of element 10. This implies that element 10 corresponds to the mutation position of the energy damage index curve. Thus, segment 10 can be considered as a defective unit. Additionally, the distance between the two parallel lines increased as the damage

Table 1 Damage conditions for the beam

damage case	element number	stiffness reduction
scenario 1	10	10%
scenario 2	10	20%
scenario 3	10	30%
scenario 4	10	40%
scenario 5	6, 15	10%, 20%
scenario 6	6, 15	30%, 40%

Table 2 Energy damage indices for damage conditions 1–4 (no noise) ( $\times 10^{-3}$ )

element number	case 1	case 2	case 3	case 4
1	0.1532	0.3446	0.5908	0.9190
2	0.1532	0.3446	0.5908	0.9190
3	0.1532	0.3446	0.5908	0.9190
4	0.1532	0.3446	0.5908	0.9190
5	0.1532	0.3446	0.5908	0.9190
6	0.1532	0.3446	0.5908	0.9190
7	0.1532	0.3446	0.5908	0.9190
8	0.1532	0.3446	0.5908	0.9190
9	0.1532	0.3446	0.5908	0.9190
10	0.0051	0.0115	0.0196	0.0305
11	-0.1384	-0.3113	-0.5337	-0.8301
12	-0.1384	-0.3113	-0.5337	-0.8301
13	-0.1384	-0.3113	-0.5337	-0.8301
14	-0.1384	-0.3113	-0.5337	-0.8301
15	-0.1384	-0.3113	-0.5337	-0.8301
16	-0.1384	-0.3113	-0.5337	-0.8301
17	-0.1384	-0.3113	-0.5337	-0.8301
18	-0.1384	-0.3113	-0.5337	-0.8301
19	-0.1384	-0.3113	-0.5337	-0.8301
20	-0.1384	-0.3113	-0.5337	-0.8301

extent of element 10 increased. Next, a random noise level of 1% was added to the deflection parameter to simulate the actual test error. The equation for simulating random noise is as follows.

$$u_i^* = u_i \cdot [1 + \varepsilon \cdot \text{unifrnd}(-1, 1)], \quad (16)$$

where  $u_i^*$  denotes the  $i$ -th contaminated displacement data,  $u_i$  denotes the  $i$ -th coefficient of the displacement vector  $u$ ,  $\varepsilon$  denotes the level of random noise, and  $unifrnd(-1,1)$  denotes a random number between  $-1$  and  $1$ . Data noise mainly reflects the adverse effects due to random fluctuations in the environmental conditions (temperature and humidity) during the measurement process. It is important to note that the measured displacement data must be multiplied by the corresponding correction coefficient when the temperature or humidity changes significantly. In this example, only small fluctuations in the environmental factors in practice were simulated by data noise. Furthermore, Fig. 6 shows the curves of the energy damage indices for damage conditions 1–4 with 1% noise. As shown in Fig. 6, the energy damage indices are slightly affected by the data error, and the defect

position (segment 10) can also be determined by inspecting the abrupt position of the curve of the graph. When data noise is considered, the mutation of the energy damage index can also be determined using the following statistical tool: (1) calculate the mean and standard deviation of the damage indices for elements 1–9 and elements 11–20, respectively; (2) calculate the deviations between the damage index of element 10 and mean values obtained in step 1; (3) compare the deviations with the standard deviations and determine whether element 10 has a mutation. The threshold for determining the mutation was set as three times the standard deviation. Tables 3 and 4 present the statistical calculation results obtained in Fig. 6 using the aforementioned steps.

Tables 3 and 4 show that element 10 can be determined as the mutation location (i.e., damage location) for

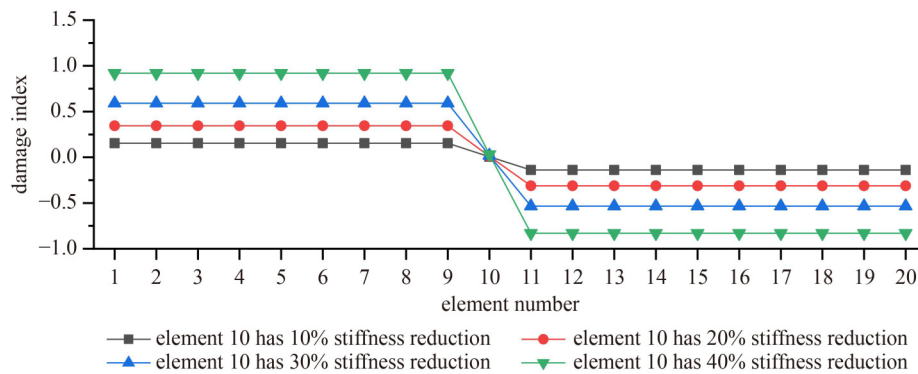


Fig. 5 Energy damage indices when element 10 is damaged (no noise).

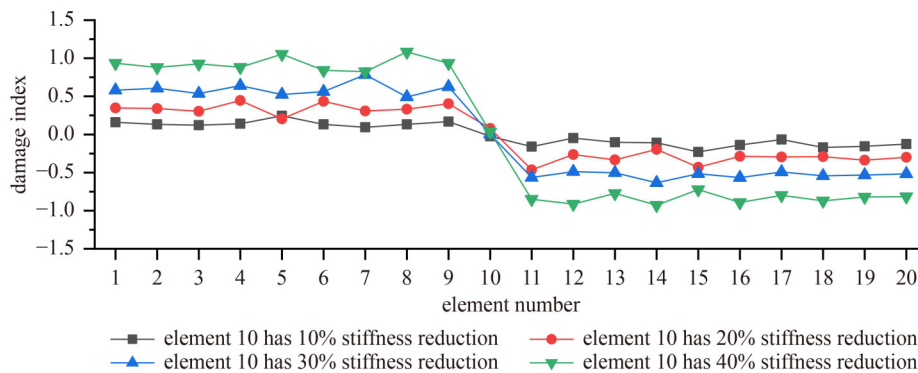


Fig. 6 Energy damage indices when element 10 is damaged (1% noise).

Table 3 Deviations between the damage index of element 10 and mean of the damage indices for elements 1–9 (1% noise)

damage case	mean of the damage indices for elements 1–9 ( $\overline{\Delta\Omega}_{1-9}$ )	standard deviation of the damage indices for elements 1–9 ( $\sigma_{1-9}$ )	$\Delta\Omega''_{10} - \overline{\Delta\Omega}_{1-9} - 3 \cdot \sigma_{1-9}$
scenario 1	0.1478	0.0423	0.0455 > 0
scenario 2	0.3468	0.0743	0.0451 > 0
scenario 3	0.5948	0.0862	0.3322 > 0
scenario 4	0.9288	0.0879	0.6326 > 0

Table 4 Deviations between the damage index of element 10 and mean of the damage indices for elements 11–20 (1% noise)

damage case	mean of the damage indices for elements 11–20 ( $\overline{\Delta\Omega}_{11-20}$ )	standard deviation of the damage indices for elements 11–20 ( $\sigma_{11-20}$ )	$\Delta\Omega''_{10} - \overline{\Delta\Omega}_{11-20} - 3 \cdot \sigma_{11-20}$
scenario 1	-0.1305	0.0529	-0.053 < 0
scenario 2	-0.32	0.0783	0.164 > 0
scenario 3	-0.5355	0.0441	0.4072 > 0
scenario 4	-0.8392	0.0649	0.6771 > 0

damage cases 2–4 because all the corresponding deviations are greater than 0. For damage case 1, element 10 can also be determined as the most probable mutation location (i.e., the most probable damage location) because the deviation between the damage index of element 10 and mean of the damage indices for elements 1–9 is greater than 0. Notably, the deviation between the damage index of element 10 and mean of the damage indices for elements 11–20 is less than zero for damage case 1. This is mainly due to the fact that the degree of damage in case 1 is very small (10% stiffness reduction). Thus, the adverse effect of data noise is relatively large in this case.

For multiple damage conditions, Figs. 7 and 8 present the curves of the energy damage indices for damage cases 5 and 6 with and without noise, respectively. As observed in Fig. 7, the energy damage indices of elements 6 and 15 significantly differ from those of the adjacent elements. This implies that elements 6 and 15 were damaged because their corresponding damage indices corresponded to the energy mutation points. When 1% noise is considered, the curves of the energy damage indices in Fig. 8 can also approximately indicate the damage locations (elements 6 and 15) based on the changes in the curve. Similarly, Tables 5–8 present the statistical calculation results obtained from Fig. 8.

Tables 5–8 show that elements 6 and 15 can be determined as the mutation locations (i.e., damage locations) for damage cases 5–6 because all the corresponding deviations are greater than 0. It can be concluded that the proposed approach is robust and successful in determining the damage position of the beam structure.

As shown in Figs. 5–8, the degree of mutation of the energy damage index is more obvious as the degree of damage increases. This implies that large damage is easier to detect using the proposed approach. Furthermore, these results demonstrate that the proposed approach can effectively detect single or multiple defects in a concrete beam structure. It is important to note that the presented algorithm can identify the significant stiffness degradation of beam-like structures. If the defect does not cause deterioration of the structural stiffness, then it is difficult to successfully determine the defect position in the beam structure using this method.

For further investigation, the applicability of the presented approach is evaluated again via a multiple-defect scenario when two damaged locations are in the neighborhood. Without loss of generality, elements 12 and 13 in the beam structure are assumed as damaged with a decrease in stiffness of 20% and 15%, respectively. Figure 9 shows the energy damage index

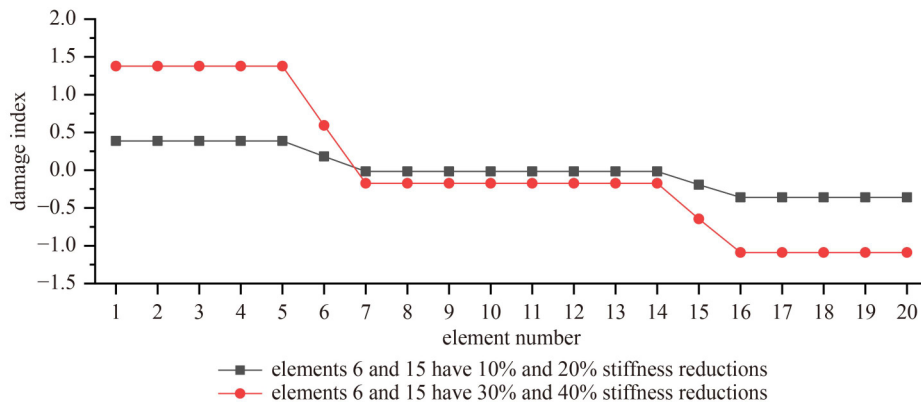


Fig. 7 Energy damage indices when elements 6 and 15 are damaged (no noise).

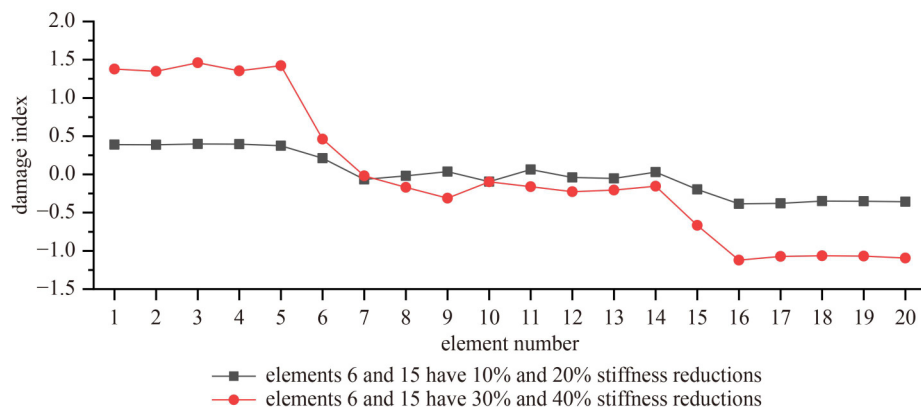


Fig. 8 Energy damage indices when elements 6 and 15 are damaged (1% noise).

curves for this adjacent damage scenario with and without 1% noise.

In Fig. 9, it can be observed that the damage indices form two parallel lines, with the exception of elements 12 and 13, when using noise-free data. This implies that only elements 12 and 13 correspond to the mutation positions

**Table 5** Deviations between the damage index of element 6 and mean of the damage indices for elements 1–5 (1% noise)

damage case	mean of the damage indices for elements 1–5 ( $\overline{\Delta\Omega}_{1-5}$ )	standard deviation of the damage indices for elements 1–5 ( $\sigma_{1-5}$ )	$\Delta\Omega_6'' - \overline{\Delta\Omega}_{1-5} - 3 \cdot \sigma_{1-5}$
case 5	0.3892	0.009	0.1512 > 0
case 6	1.3926	0.0478	0.7871 > 0

**Table 6** Deviations between the damage index of element 6 and mean of the damage indices for elements 7–14 (1% noise)

damage case	mean of the damage indices for elements 7–14 ( $\overline{\Delta\Omega}_{7-14}$ )	standard deviation of the damage indices for elements 7–14 ( $\sigma_{7-14}$ )	$\Delta\Omega_6'' - \overline{\Delta\Omega}_{7-14} - 3 \cdot \sigma_{7-14}$
case 5	-0.0176	0.0558	0.0612 > 0
case 6	-0.1671	0.0867	0.3692 > 0

**Table 7** Deviations between the damage index of element 15 and mean of the damage indices for elements 7–14 (1% noise)

damage case	mean of the damage indices for elements 7–14 ( $\overline{\Delta\Omega}_{7-14}$ )	standard deviation of the damage indices for elements 7–14 ( $\sigma_{7-14}$ )	$\Delta\Omega_{15}'' - \overline{\Delta\Omega}_{7-14} - 3 \cdot \sigma_{7-14}$
case 5	-0.0176	0.0558	0.0109 > 0
case 6	-0.1671	0.0867	0.2392 > 0

**Table 8** Deviations between the damage index of element 15 and mean of the damage indices for elements 16–20 (1% noise)

damage case	mean of the damage indices for elements 16–20 ( $\overline{\Delta\Omega}_{16-20}$ )	standard deviation of the damage indices for elements 16–20 ( $\sigma_{16-20}$ )	$\Delta\Omega_{15}'' - \overline{\Delta\Omega}_{16-20} - 3 \cdot \sigma_{16-20}$
case 5	-0.3641	0.165	0.1187 > 0
case 6	-1.0845	0.0233	0.3482 > 0

of the energy damage index curve. Thus, elements 12 and 13 can be determined as damaged units. When data noise is considered, the corresponding curve in Fig. 9 also approximately indicates that elements 12 and 13 are the damage locations. Using the statistical tool stated earlier, Tables 9 and 10 list the statistical deviations of the energy damage indices for elements 12 and 13. In Tables 9 and 10, it can be observed that elements 12 and 13 can be determined as the mutation locations (i.e., damage locations) because all the corresponding deviations are greater than 0. It can be concluded that the proposed algorithm is also applicable to the adjacent damage scenario of the beam structure.

## 4 Experimental verifications of the proposed method

### 4.1 Channel steel beam

An experimental steel beam conducted by Le et al. [45] is used to verify the proposed approach. This channel steel beam is subdivided into five elements, and six displacement meters are used to acquire the deflection data under mid-span loading. The overall length of the steel beam channel was 2475 mm. The damage was simulated by cutting part of the steel beam, and the cutting position was 1175 mm away from the left support. The specific process of the static test and the measured deflection data of the intact and damaged structures can be found in Ref. [45].

The MATLAB software was used to implement the proposed method for this experimental example on a computer. Using the measured deflection data, the elemental damage index  $\Delta\Omega_i''$  can be directly calculated using Eq. (15) without constructing the beam FEM. Table 11 presents the calculated values of  $\Delta\Omega_i''$ . The corresponding damage index curve does not need to be drawn because this example is very simple. From Table 11, it can be observed that the damage indices of segments 1 and 2 are very close, and the damage indices

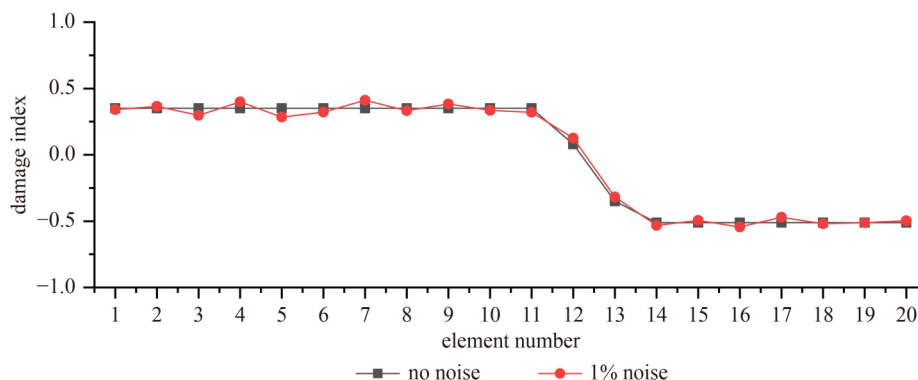


**Fig. 9** Energy damage indices when elements 12 and 13 are damaged.

**Table 9** Deviation between the damage index of element 12 and mean of the damage indices for elements 1–11 (1% noise)

number	mean of the damage indices for elements 1–11 ( $\overline{\Delta\Omega}_{1-11}$ )	standard deviation of the damage indices for elements 1–11 ( $\sigma_{1-11}$ )	$\Delta\Omega''_{12} - \overline{\Delta\Omega}_{1-11} - 3 \cdot \sigma_{1-11}$
element 12	0.3447	0.0408	0.0969 > 0

**Table 10** Deviation between the damage index of element 13 and the mean of the damage indices for elements 14–20 (1% noise)

number	mean of the damage indices for elements 14–20 ( $\overline{\Delta\Omega}_{14-20}$ )	standard deviation of the damage indices for elements 14–20 ( $\sigma_{14-20}$ )	$\Delta\Omega''_{13} - \overline{\Delta\Omega}_{14-20} - 3 \cdot \sigma_{14-20}$
element 13	-0.5098	0.0250	0.1164 > 0

**Table 11** Damage indices for the channel steel beam

segment number (left-to-right)	damage index
1	0.0015
2	0.0014
3	-0.0002
4	-0.0014
5	-0.0013

of segments 4 and 5 are also very close. Only the damage index of segment 3 showed a mutation. In other words, the energy damage index of element 3 is significantly different from that of the adjacent elements. Therefore, it can be concluded that segment 3 is damaged. This is in line with the real situation in which segment 3 has a gap caused by cutting. It can be concluded that the proposed algorithm is a simple and practical defect-localization method.

It should be noted that the damage localization accuracy of the proposed approach is closely related to the spacing of the displacement sensors. The smaller the distance between the displacement sensors, the higher is the accuracy of damage localization. For this experimental beam, based on the above judgment that the defect is located at segment 3, the defect location can be accurately determined by arranging more displacement sensors only in segment 3 of the beam. In other words, by adjusting the position of the displacement sensor step by step, the proposed method can be operated several times until satisfactory damage localization results are obtained. Because the sensor position is not adjusted in Ref. [45], the proposed method can only detect that the damage is located in segment 3 at the present stage. In future research, an improved method based on a step-by-step arrangement of displacement sensors should be investigated to achieve more precise defect localization results.

#### 4.2 Concrete beam with rectangular cross section

A concrete beam with a rectangular cross-section

conducted by Lu [46] was used to verify the proposed method. This concrete beam is subdivided into eight elements, and seven displacement meters are used to collect the deflection data under two-point loading. The actual span of the concrete beam is 2000 mm. The damage state was simulated by gradually increasing the static load to crack the concrete beam. The specific physical properties of the beam and the measured deflection data of the static test can be found in Ref. [46]. The deflection data of the beam under two loading conditions (load = 30 kN and load = 45 kN) were measured in the experiment. When load = 30 kN, the concrete beam was in the normal working condition. When load = 45 kN, there was evident crack damage in the mid-span area of this beam.

Using these deflection data, the damage status of the concrete beam was evaluated using the proposed approach. For the calculation of  $\Delta\Omega''$ , the beam deflection data under a load of 45 kN should be scaled to the data under a load of 30 kN because  $\Delta\bar{u}$  is the displacement change for a structure under the same load. The deflection data transformation from 45 to 30 kN were obtained according to the load proportion. In other words, the converted deflection data is calculated by multiplying the measured data under the load of 45 kN with the load proportion of 30/45. It is important to note that this treatment of the data transformation from 45 to 30 kN is a type of simplification because there is no strict linear relation between the force and displacement when the beam is cracked. Subsequently, the elemental damage index  $\Delta\Omega''_i$  can be directly calculated using Eq. (15) without constructing the beam FEM. Table 12 lists the calculated values of  $\Delta\Omega''_i$ . As shown in Table 12, only the damage indices of segments 4 and 5 exhibited obvious mutations. Similar to the numerical example, the mutation of the energy damage index can also be determined using the statistical calculation results as shown in Tables 13 and 14. It can be concluded from Tables 13 and 14 that segments 4 and 5 can be determined as mutation locations (i.e., damage locations) because their corresponding deviations are greater than 0. This is in line with the actual crack locations (segments 4 and 5) observed in the experiment. It can be concluded that the proposed algorithm is effective for damage detection in experimental concrete beams.

## 5 Conclusions

A static strain energy redistribution approach was developed for defect evaluation of beam-like structures. The proposed approach uses spectral decomposition of the elemental stiffness matrix and deflection variation of a beam. For energy release, the static strain energy of a beam is redistributed in each beam segment when

**Table 12** Damage indices for the experimental concrete beam ( $\times 10^{-4}$ )

segment number	damage index
1	0.6853
2	0.6973
3	0.7267
4	-0.2040
5	-0.1787
6	-0.5200
7	-0.5960
8	-0.6107

**Table 13** Deviations between the damage index of segment 4 and mean of the damage indices for segments 1–3 of the experimental concrete beam

number	mean of the damage indices for elements 1–3 ( $\overline{\Delta\Omega}_{1-3}$ )	standard deviation of the damage indices for elements 1–3 ( $\sigma_{1-3}$ )	$\Delta\Omega_4'' - \overline{\Delta\Omega}_{1-3}$ $-3 \cdot \sigma_{1-3}$
segment 4	$7.0311 \times 10^{-5}$	$2.1264 \times 10^{-6}$	$8.4332 \times 10^{-5} > 0$

**Table 14** Deviations between the damage index of segment 5 and mean of the damage indices for segments 6–8 of the experimental concrete beam

number	mean of the damage indices for elements 6–8 ( $\overline{\Delta\Omega}_{6-8}$ )	standard deviation of the damage indices for elements 6–8 ( $\sigma_{6-8}$ )	$\Delta\Omega_5'' - \overline{\Delta\Omega}_{6-8}$ $-3 \cdot \sigma_{6-8}$
segment 5	$-5.7556 \times 10^{-5}$	$4.8668 \times 10^{-6}$	$2.5088 \times 10^{-5} > 0$

structural damage occurs. This implies that the static strain energy of the defect in a beam will exhibit a mutation. Alternatively, the static energy variation can serve as an index for determining the position of the defect in a beam. The remarkable advantage of the developed method is that it can be used for defect detection with simple calculations and fast operation even if the structural FEM is not constructed in advance. The proposed damage-detection approach was validated using numerical and experimental beam structures. Based on the calculation results, the following conclusions were drawn.

1) For an intact structure with no damage, the shear energy damage index is equal to zero, and the corresponding damage index graph is a horizontal line.

2) For the damaged structure, the shear energy damage index suddenly changes at the damage location, and the corresponding damage index curve corresponds to a stepped broken line. Based on the obtained results, it can be concluded that the location of the shear energy mutation is the exact location of the damaged element in the beam structure.

3) When the deflection data of the beam are contaminated, the damage location can also be determined using a statistical tool. The threshold to determine the mutation associated with the damage

location can be set as thrice the standard deviation of the energy damage indices.

4) The damage localization precision of this algorithm is closely related to the spacing between the displacement sensors. As the distance between the displacement sensors decreases, the accuracy of damage localization increases. In practice, the proposed method can be operated several times by adjusting the position of the displacement sensor until satisfactory damage localization results are obtained.

Furthermore, the proposed approach has several limitations. The precondition for the application of the proposed method is that the beam structure must exhibit detectable displacement changes before and after the damage. This implies that this method is accurate when the stiffness reduction is significant with a detectable displacement change. Additionally, this method cannot be used to determine the severity of damaged elements. When the damage location is determined by the proposed method, other parameter identification methods, such as optimization algorithms, can be further employed to calculate the degree of damage. In future studies, the applicability of this approach to other types of structures can be examined to expand its application scope. Although this approach has been demonstrated via numerical and experimental cases, it is still necessary to conduct further engineering case verification studies in the future.

**Acknowledgments** This study was supported by the National Natural Science Foundation of Zhejiang Province, China (No. LQ20E080013), the Natural Science Foundation of China (Grant No. 52008215), the Major Special Science and Technology Project (No. 2019B10076) of “Ningbo Science and Technology Innovation 2025” and Ningbo Natural Science Foundation Project (No. 202003N4169).

## References

- Doebbling S W, Farrar C R, Prime M B. A summary review of vibration-based damage identification methods. *Shock and Vibration Digest*, 1998, 30(2): 91–105
- Carden E P, Fanning P. Vibration based condition monitoring: A review. *Structural Health Monitoring*, 2004, 3(4): 355–377
- Prinaris A, Alampalli S, Ettouney M. Review of Remote Sensing for Condition Assessment and Damage Identification after Extreme Loading Conditions. Vancouver: Structures Congress 2008, ASCE, 2008
- Liu G, Wang L, Liu J K, Chen Y M, Lu Z R. Identification of an airfoil-store system with cubic nonlinearity via enhanced response sensitivity approach. *AIAA Journal*, 2018, 56(12): 4977–4987
- Liu G, Wang L, Luo W L, Liu J K, Lu Z R. Parameter identification of fractional order system using enhanced response sensitivity approach. *Communications in Nonlinear Science and Numerical Simulation*, 2019, 67(2): 492–505
- Messina A, Williams J E, Contursi T. Structural damage detection

- by a sensitivity and statistical-based method. *Journal of Sound and Vibration*, 1998, 216(5): 791–808
7. Ashokkumar C R, Iyengar N G R. Partial eigenvalue assignment for structural damage mitigation. *Journal of Sound and Vibration*, 2011, 330(1): 9–16
  8. Yang Z, Wang L. Structural damage detection by changes in natural frequencies. *Journal of Intelligent Material Systems and Structures*, 2010, 21(3): 309–319
  9. Shi Z Y, Law S S, Zhang L M. Damage localization by directly using incomplete mode shapes. *Journal of Engineering Mechanics*, 2000, 126(6): 656–660
  10. Ghannadi P, Kourehli S S. Investigation of the accuracy of different finite element model reduction techniques. *Structural Monitoring and Maintenance*, 2018, 5(3): 417–428
  11. Ghannadi P, Kourehli S S. Data-driven method of damage detection using sparse sensors installation by SEREPa. *Journal of Civil Structural Health Monitoring*, 2019, 9(4): 459–475
  12. Ghannadi P, Kourehli S S. An effective method for damage assessment based on limited measured locations in skeletal structures. *Advances in Structural Engineering*, 2021, 24(1): 183–195
  13. Ghannadi P, Kourehli S S, Noori M, Altabay W A. Efficiency of grey wolf optimization algorithm for damage detection of skeletal structures via expanded mode shapes. *Advances in Structural Engineering*, 2020, 23(13): 2850–2865
  14. Ghannadi P, Kourehli S S. Prediction of unmeasured mode shapes and structural damage detection using least squares support vector machine. *Structural Monitoring and Maintenance*, 2018, 5(3): 379–390
  15. Zhu H P, Li L, He X Q. Damage detection method for shear buildings using the changes in the first mode shape slopes. *Computers & Structures*, 2011, 89(9–10): 733–743
  16. Zhang Y, Wang L, Xiang Z. Damage detection by mode shape squares extracted from a passing vehicle. *Journal of Sound and Vibration*, 2012, 331(2): 291–307
  17. Wu D, Law S S. Model error correction from truncated modal flexibility sensitivity and generic parameters. I: Simulation. *Mechanical Systems and Signal Processing*, 2004, 18(6): 1381–1399
  18. Di W, Law S S. Eigen-parameter decomposition of element matrices for structural damage detection. *Engineering Structures*, 2007, 29(4): 519–528
  19. Yang Q W, Liu J K. Damage identification by the eigenparameter decomposition of structural flexibility change. *International Journal for Numerical Methods in Engineering*, 2009, 78(4): 444–459
  20. Yang Q W. A new damage identification method based on structural flexibility disassembly. *Journal of Vibration and Control*, 2011, 17(7): 1000–1008
  21. Sung S H, Jung H J, Jung H Y. Damage detection for beam-like structures using the normalized curvature of a uniform load surface. *Journal of Sound and Vibration*, 2013, 332(6): 1501–1519
  22. Yang Z B, Radzienski M, Kudela P, Ostachowicz W. Fourier spectral-based modal curvature analysis and its application to damage detection in beams. *Mechanical Systems and Signal Processing*, 2017, 84: 763–781
  23. Xiang J, Matsumoto T, Wang Y, Jiang Z. Detect damages in conical shells using curvature mode shape and wavelet finite element method. *International Journal of Mechanical Sciences*, 2013, 66: 83–93
  24. Khorram A, Bakhtiari-Nejad F, Rezaeian M. Comparison studies between two wavelet based crack detection methods of a beam subjected to a moving load. *International Journal of Engineering Science*, 2012, 51: 204–215
  25. Roveri N, Carcaterra A. Damage detection in structures under traveling loads by Hilbert–Huang transform. *Mechanical Systems and Signal Processing*, 2012, 28: 128–144
  26. Cavadas F, Smith I F C, Figueiras J. Damage detection using data-driven methods applied to moving-load responses. *Mechanical Systems and Signal Processing*, 2013, 39(1–2): 409–425
  27. Xu Z D, Liu M, Wu Z, Zeng X. Energy damage detection strategy based on strain responses for long-span bridge structures. *Journal of Bridge Engineering*, 2011, 16(5): 644–652
  28. Yi T H, Li H N, Sun H M. Multi-stage structural damage diagnosis method based on “energy-damage” theory. *Smart Structures and Systems*, 2013, 12(3–4): 345–361
  29. Cha Y J, Buyukozturk O. Structural damage detection using modal strain energy and hybrid multiobjective optimization. *Computer-Aided Civil and Infrastructure Engineering*, 2015, 30(5): 347–358
  30. Ghannadi P, Kourehli S S. Structural damage detection based on MAC flexibility and frequency using moth-flame algorithm. *Structural Engineering and Mechanics*, 2019, 70(6): 649–659
  31. Ghannadi P, Kourehli S S. Model updating and damage detection in multi-story shear frames using Salp Swarm Algorithm. *Earthquakes and Structures*, 2019, 17(1): 63–73
  32. Ghannadi P, Kourehli S S. Multiverse optimizer for structural damage detection: Numerical study and experimental validation. *Structural Design of Tall and Special Buildings*, 2020, 29(13), e1777: 1–27
  33. Ghannadi P, Kourehli S S. Efficiency of the slime mold algorithm for damage detection of large-scale structures. *Structural Design of Tall and Special Buildings*, 2022, e1967: 1–36
  34. Wang X, Hu N, Fukunaga H, Yao Z H. Structural damage identification using static test data and changes in frequencies. *Engineering Structures*, 2001, 23(6): 610–621
  35. Sanayei M, Onipede O. Assessment of structures using static test data. *AIAA Journal*, 1991, 29(7): 1174–1179
  36. Banan M R, Banan M R, Hjelmstad K D. Parameter estimation of structures from static response, I: Computational aspects. *Journal of Structural Engineering*, 1994, 120(11): 3243–3258
  37. Banan M R, Banna M R, Hjelmstad K D. Parameter estimation of structures from static response, II: Numerical simulation studies. *Journal of Structural Engineering*, 1994, 120(11): 3259–3283
  38. Hjelmstad K D, Shin S. Damage detection and assessment of structures from static response. *Journal of Engineering Mechanics*, 1997, 123(6): 568–576
  39. Chou J H, Ghaboussi J. Genetic algorithm in structural damage detection. *Computers & Structures*, 2001, 79(14): 1335–1353
  40. Bakhtiari-Nejad F, Rahai A, Esfandiari A. A structural damage detection method using static noisy data. *Engineering Structures*, 2005, 27(12): 1784–1793
  41. Chen X, Zhu H, Chen C. Structural damage identification using

- test static data based on grey system theory. *Journal of Zhejiang University. Science A*, 2005, 6(8): 790–796
42. Kouchmeshky B, Aquino W, Bongard J C, Lipson H. Co-evolutionary algorithm for structural damage identification using minimal physical testing. *International Journal for Numerical Methods in Engineering*, 2007, 69(5): 1085–1107
  43. Abdo M A B. Parametric study of using only static response in structural damage detection. *Engineering Structures*, 2012, 34: 124–131
  44. Abdo M A B. Corrigendum to “Parametric study of using only static response in structural damage detection” [*Engineering Structures* 34 (2012) 124–131]. *Engineering Structures*, 2012, 35: 322
  45. Le N T, Thambiratnam D P, Nguyen A, Chan T H T. A new method for locating and quantifying damage in beams from static deflection changes. *Engineering Structures*, 2019, 180: 779–792
  46. Lu Y. Random beam structure damage identification method based on static measurement data and L1 regularization. Thesis for the Master’s Degree. Wuhan: Wuhan University of Technology, 2019 (in Chinese)